TECHNICAL RESEARCH REPORT

Analysis of Heat Transfer in a Chemical Vapor Deposition Reactor: An Eigenfunction Expansion Solution Approach

by Hsiao-Yung Chang,
Raymond A. Adomaitis

T.R. 97-84

Sponsored by
the National Science Foundation
Engineering Research Center Program,
the University of Maryland,
Harvard University,
and Industry

Analysis of Heat Transfer in a Chemical Vapor Deposition Reactor: An Eigenfunction Expansion Solution Approach

Hsiao-Yung Chang and Raymond A. Adomaitis

Department of Chemical Engineering and Institute for System Research,

University of Maryland, College Park, MD 20742

Abstract

A numerical solution procedure combining several weighted residual methods and based on global trial function expansion is developed to solve a model for the steady state gas flow field and temperature distribution in a low-pressure chemical vapor deposition reactor. The enthalpy flux across wafer/gas boundary is calculated explicitly and is found to vary significantly as a function of wafer position. An average heat transfer coefficient is estimated numerically and is compared to typical radiative heat transfer rates in these system. The convergence properties of the discretization method developed are also discussed.

Keywords chemical vapor deposition; eigenfunction expansion; weighted residual methods; collocation

Introduction

Chemical vapor deposition (CVD) is a technique extensively used in the semiconductor industry to form nonvolatile solid films on a substrate from chemical reactions fed by vapor phase reactants. The quality of the film, e.g., the thickness, composition, and microstructure, is a critical manufacturing requirement. Moreover, the film quality must be reproducible and uniform within each wafer itself and from wafer to wafer in a processing batch.

Temperature, along with pressure, position, and reactant gas composition, is one of the most important factors in high-quality deposition processes. Because the deposition reaction is initiated when the vapor phase reactants receive sufficient energy from the wafer surface or other heat sources, a detailed temperature distribution profile, including gas phase and wafer, is required for a complete process model. This temperature information also can be used to design and control the reactor to operate at processing conditions that reduce unwanted gas phase reactions which might result in particle contamination.

There is a large literature on the mathematical modeling and simulation of different CVD systems. Kleijn (1995) provides an overview of these modeling issues. Middlemann and Hochberg (1993) discuss different modeling aspects from a chemical engineering viewpoint, and Badgwell et. al. (1995) summarized some modeling and control issues in CVD. Most published CVD system models are solved numerically, either by the finite volume method (Kleijn et. al. 1991), finite element method (Moffat and Jensen 1988), or finite difference method (Duverneuil and Couderc 1992). These discretization methods are based on spatially-localized trial functions, and are well-suited for solving problems with irregular geometries. The large number of algebraic or differential equations that are generated by these discretization procedures, however, may make the resulting simulations inappropriate to use in real-time control applications or interative optimization methods. On the other hand, those models sufficiently simple to be solved explicitly may be incapable of resolving important physical features.

In this work, we develop an analytical approximation solution based on global trial functions to solve a combined set of CVD system gas flow and temperature modelling equations. This choice was motivated by the excellent convergence properties of spectral methods (Gottlieb and Orszag 1977), and the clear connections that remain during the solution procedure between model parameters and the solution behavior. We see our approach as a method intermediate between the finite element and explicit solution procedures, an analysis method particularly well-suited to distinguishing factors which may require more detailed simulation from those which can be identified as unimportant.

For the CVD system studied, the gas flow field is solved first using a Galerkin projection on a set of globally-defined polynomial trial functions. We then use a two-dimensional eigenfunction expansion method, conjugated with a one-point collocation discretization in the spanwise direction, to compute the three-

dimensional gas temperature profile. The heat transfer rate at the wafer surface is calculated explicitly from the eigenfunction expansion solution. Heat transfer rates from the wafer to the gas phase are shown to be significant when compare to radiative heat transfer.

Model Formulation

The CVD system

The BTU-ULVAC ERA-1000 selective tungsten deposition system is the CVD reactor to be considered in this modeling study. The geometry and dimensions of this commercially manufactured, single-wafer, cold-wall reactor are shown in Figure 1. Reactant gases are fed to the reactor from two sources: a gas mixture of silane, tungsten hexafluoride, and argon carrier gas is injected through a two-dimensional nozzle installed on one side wall, and hydrogen is pumped in through a transparent showerhead mounted in the top of the reactor chamber. Gases mix in the chamber and react at the surface of a 4 inch wafer located at the chamber center. The wafer is supported by a slowly rotating 0.16 m diameter quartz susceptor and the wafer edge is covered by a quartz guard ring to help reduce edge heat loss. This leaves a 0.076 m diameter area of wafer surface exposed to reaction. An incoherent tungsten-halogen lamp ring is used to heat the wafer to 300^oC through the transparent showerhead. Typical deposition runtimes last 5 minutes after operating temperature is reached.

Gas Flow Field

Although gas feed enters from both the showerhead and side slits, we will only consider the case where the gas flow field over the wafer is assumed to be dominated by the horizontal flow, generated by the feed gas entering through the side wall nozzle. Arectangular pipe flow model is assumed for the reactant gas mixture. The fully developed, laminar velocity profile is obtained by solving steady state momentum conservation Navier-Stokes and continuity equations. The transport and gas thermodynamic properties are assumed constant and evaluated at the reference temperature T_{amb}. It is also assumed the gas heating effect near the wafer surface and the slow wafer rotation do not affect the flow field. The governing equations for the flow

field component in the x direction are written as

$$\frac{\partial v_x}{\partial x} = 0$$

$$\frac{\partial^2 v_x}{\partial y^2} + \alpha_v \frac{\partial^2 v_x}{\partial z^2} = \beta_v.$$

The dimensionless pressure drop term $\beta_v = 2\mathcal{P}\overline{Y}^2/(\mu < v > \overline{X})$ can only be determined after the flow field equations are solved. Thus, defining the flow velocity/pressure drop ratio as $\hat{v}_x = v_x/\beta_v$, the momentum balance equation can be rewritten as

$$\frac{\partial^2 \hat{v}_x}{\partial y^2} + \alpha_v \frac{\partial^2 \hat{v}_x}{\partial z^2} = 1 \tag{1}$$

subject to no-slip boundary conditions at $y = 0, 1$ and $z = 0, 1$.

Gas Temperature Field

Neglecting heat generated by viscous dissipation and the gas phase chemical reactions, the gas phase energy balance equation gives

$$v_x \frac{\partial T_g}{\partial x} = \delta_{gt} \frac{\partial^2 T_g}{\partial x^2} + \beta_{gt} \frac{\partial^2 T_g}{\partial y^2} + \gamma_{gt} \frac{\partial^2 T_g}{\partial z^2}. \tag{2}$$

Gas temperature boundary conditions are based on assuming the showerhead temperature equals the chamber wall temperature and that the convective heat transfer dominates at the reactor gas outlet. Gas temperature is set equal to the wafer/susceptor temperature T_w inside the region of radius R_2 at $z = 0$, and to the wall temperature T_{wall} outside this region:

$$\begin{aligned}
T_g &= 0 \qquad \text{at } x = 0 \\
\frac{\partial T_g}{\partial x} &= 0 \qquad \text{at } x = 1 \\
T_g &= C_1(T_{wall}) \qquad \text{at } y = 0, 1 \\
T_g &= C_1(T_{wall}) \qquad \text{at } z = 1 \\
T_g &= \begin{cases} C_2(T_w) & \text{at } z = 0, \quad (x - 0.5)^2 + R_1^2(y - 0.5)^2 \leq R_2^2 \\ C_1(T_{wall}) & \text{at } z = 0, \quad R_2^2 < (x - 0.5)^2 + R_1^2(y - 0.5)^2. \end{cases}
\end{aligned}$$

In the above equations, the following dimensionless parameters and variables are used: $x = x^*/2\overline{X}$; $y = y^*/2\overline{Y}$; $z = z^*/2\overline{Z}$; $v_x = v_x^*/< v >$; $T_g = (T_g^* - T_{amb})/T_{amb}$; $T_w = T_w^*/T_{amb}$; $T_{wall} = T_{wall}^*/T_{amb}$. Here, T_{amb} is the inlet gas temperature and $< v >$ is average gas entrance velocity. Parameters C_1 and C_2 are defined as $(T_{wall} - T_{amb})/T_{amb}$ and $(T_w - T_{amb})/T_{amb}$, respectively. The aspect ratio is $R_1 = \overline{Y}/\overline{X}$ and the radius of wafer/susceptor is $R_2 = R_s/2\overline{X}$. For the special case where the chamber wall temperature is set equal to constant inlet ambient temperature, the wafer/susceptor becomes the only heat source in the system and $C_1 = 0$, giving homogeneous boundary conditions at all boundaries except $z = 0$.

Representative process operating conditions correspond to a feed volumetric flow rate of 250 sccm, a feed gas temperature of 298K and mixture ratio of $WF_6/SiH_4/Ar$ equals to 1/1/23, chamber pressure of 0.5 torr, and a uniform wafer temperature of 313 ^{o}C. The gas mixture density ρ, thermal conductivity κ, heat capacity C_p, and viscosity μ are mixture-averaged properties (Kee et. al. 1986) and the pure species viscosities are calculated from the kinetic theorey of gases at reference temperature T_{amb}. The value of dimensionless parameters are given in Table 1.

Flow Field Solution

A Galerkin technique is used to compute the flow field velocity component v_x as a function of y and z. We choose the trial functions η_{ij} to satisfy the no slip boundary conditions and continuity equation by definition,

$$\eta_{ij} = (y^i - y^{i+1})(z^j - z^{j+1}) \qquad i=1, \ldots ,\mathrm{I}, \quad j=1, \ldots ,\mathrm{J} \tag{3}$$

and normalize this sequence with a numerical Gram-Schmidt orthonormalization procedure to define the trial function ξ_{ij}. The residual formed by substituting the truncated series expansion approximation $v_x = \sum_{i,j=1}^{I,J} d_{ij}\xi_{ij}$ into (1) to obtain

$$\mathcal{R}_v = \sum_{i,j=1}^{I,J} d_{ij}(\nabla_y^2 \xi_{ij} + \alpha_v \nabla_z^2 \xi_{ij}) - 1. \tag{4}$$

The mode amplitude coefficients d_{ij} are computed by minimizing the residual with the Galerkin projection, i.e., projecting the residual onto each trial function ξ_{mn}:

$$\sum_{i,j=1}^{I,J} d_{ij} \langle (\nabla_y^2 + \alpha_v \nabla_z^2)\xi_{ij}, \xi_{mn} \rangle = \langle 1, \xi_{mn} \rangle \qquad m=1, \ldots ,\mathrm{I}, \quad n=1, \ldots ,\mathrm{J} \tag{5}$$

where the inner product is defined as

$$\langle f, g \rangle = \int_0^1 \int_0^1 fg \quad dydz.$$

The flow field computed by this procedure is shown in Figure 2.

The dimensionless parameter β_v and characteristic pressure drop $\mathcal{P}$ can be recovered from the numerically computed solution. Because $v_x =< v > v_x^* = \beta_v < v > \hat{v}_x$, the volumetric flow rate equals the dimensionless flow velocity integrated over the unit domain multiplied by the true area of the cross section $A_{yz} = 4\overline{YZ}$:

$$\int_0^{2\overline{Z}} \int_0^{2\overline{Y}} v_x^* dy^* dz^* = 4\overline{YZ} < v > \int_0^1 \int_0^1 \hat{v}_x dydz$$

Using the definition of average velocity, $< v >= \int_{A_{yz}} v \; dydz \; / A_{yz}$,

$$\beta_v = \left(\int_0^1 \int_0^1 \hat{v}_x dydz \right)^{-1}$$

$$\mathcal{P} = \frac{\mu < v > \overline{X}}{2\overline{Y}^2} \beta_v = 0.0402 \quad \text{Pa} \quad \text{or} \quad 0.3015 \quad \text{mtorr.}$$

Under some circumstances this Galerkin procedure generates accurate results with a single term in the series (MacCluer 1994). This is true in our system in the z direction, but it is not valid in y direction because of the high aspect ratio of the system. The comparisons are shown in Figure 3. Since the flow field is flat over the range of y most critical to our heat transfer calculations (the region containing the heated wafer and susceptor), the simplified flow field expression, $v_x(y, z) = 4v_{max}z(1 - z)$ will be used for the temperature field computations.

Gas Temperature Eigenfunction Expansion Solution

The first step in computing a solution to the gas temperature model by an eigenfunction expansion technique is to define two separate gas temperature trial function expansions. The first is used to minimize the temperature equation residual inside the reactor gas domain (T_Ω) and the second is to express the effect of the nonhomogeneous boundary condition on the temperature field ($T_{\partial\Omega}$):

$$T_g = T_\Omega + T_{\partial\Omega}. \tag{6}$$

The trial functions of each series are defined by the product of three individual functions corresponding to each direction over the physical domain shown in Figure 1

$$T_g = \sum_{l,m,n=1}^{L,M,N} b_{lmn}\phi_l(x)\psi_m(y)\zeta_n(z) + \sum_{l,m=1}^{L,M} a_{lm}\phi_l(x)\psi_m(y)\zeta_0(z).$$

In the above equation, b_{lmn} and a_{lm} are mode amplitude coefficients, ϕ_l, ψ_m, and ζ_n are trial function components in the three physical directions, and ζ_0 is chosen to not vanish at $z = 0$.

The solution procedure developed combines collocation discretization in the spanwise (y) direction and an eigenfunction expansion in the (x, z) planes defined at each collocation point y_m. The solution approximates the governing equation at each collocation position and the three dimensional results can be reconstructed even when a single interior collocation point is used.

Writing the collocation-discretized trial function expansion,

$$T_g(x, y_m, z) = \psi(y_m) \sum_{l,n=1}^{L,N} b_{lmn}\phi_l(x)\zeta_n(z) + \psi(y_m) \sum_{l=1}^{L} a_{lm}\phi_l(x)\zeta_0(z) \quad m = 1, \ldots, \mathrm{M} \tag{7}$$

where $\psi(y_m)$ is the scalar value of trial function ψ at the m-th collocation point.

The trial function components $\phi(x)$ and $\zeta(z)$ are computed from the eigenfunctions of the heat equation subject to homogeneous boundary conditions, i.e., solving for nontrivial solutions to

$$\delta_{gt}\frac{\partial^2 T_\Omega}{\partial x^2} + \gamma_{gt}\frac{\partial^2 T_\Omega}{\partial z^2} = -\lambda T_\Omega \tag{8}$$

where λ is the eigenvalue, subject to boundary condition $T_\Omega = 0$ at $z = 0, 1$ and $x = 0$, and $\partial T_\Omega/\partial x = 0$ at $x = 1$. Applying the separation of variables technique to (8), the eigenfunctions and eigenvalues are calculated as

$$\begin{aligned} \phi_l(x) &= \sin\left(\frac{2l-1}{2}\pi x\right) \\ \zeta_n(z) &= \sin(n\pi z) \\ \lambda_{ln} &= \left[\delta_{gt}\frac{(2l-1)^2}{4} + \gamma_{gt}n^2\right]\pi^2 \end{aligned} \tag{9}$$

and so the T_Ω trial function expansion contribution to the temperature field is given by the eigenfunction expansion

$$T_\Omega = \psi(y_m) \sum_{l,n=1}^{L,N} b_{lmn} \sin\left(\frac{2l-1}{2}\pi x\right) \sin(n\pi z). \tag{10}$$

Defining $\zeta_0 = 1 - z$, $T_{\partial\Omega}$ can be represented as

$$T_{\partial\Omega} = \psi(y_m) \sum_{l=1}^{L} a_{lm} \sin\left(\frac{2l-1}{2}\pi x\right)(1-z). \tag{11}$$

The nonhomogeneous boundary condition (3), denoted as $T_{g,z=0}$, is projected onto the trial functions (11) evaluated at $z = 0$ to determine the coefficients a_{lm}:

$$\psi(y_m) \sum_{l=1}^{L} a_{lm} \int_0^1 \phi_l(x)\phi_i(x)dx = \int_{1/2-R_2}^{1/2+R_2} T_{g,z=0}\phi_i(x)dx$$

and so

$$a_{lm} = \frac{8C_2}{(2l-1)\pi}\psi(y_m)\sin(\frac{2l-1}{4}\pi)\sin(\frac{2l-1}{2}\pi R_2)$$

Substituting the trial function expansion (6) into the heat equation (2) defines the residual:

$$\begin{aligned}\mathcal{R} &= \left(\delta_{gt}\frac{\partial^2 T_\Omega}{\partial x^2} + \gamma_{gt}\frac{\partial^2 T_\Omega}{\partial z^2}\right) + \left(\delta_{gt}\frac{\partial^2 T_{\partial\Omega}}{\partial x^2} + \gamma_{gt}\frac{\partial^2 T_{\partial\Omega}}{\partial z^2} - v_x(y,z)\frac{\partial T_{\partial\Omega}}{\partial x}\right) \\ &\quad -v_x(y,z)\frac{\partial T_\Omega}{\partial x} + \beta_{gt}\frac{\partial^2 T_\Omega}{\partial y^2} + \beta_{gt}\frac{\partial^2 T_{\partial\Omega}}{\partial y^2}\end{aligned}$$

At the m-th collocation point in y direction

$$\begin{aligned}\mathcal{R}(x,y_m,z) &= \sum_{l,n=1}^{L,N} b_{lmn}\psi(y_m)\left(\delta_{gt}\frac{d^2\phi_l}{dx^2}\zeta_n + \gamma_{gt}\phi_l\frac{d^2\zeta_n}{dz^2}\right) + \sum_{l=1}^{L} a_{lm}\psi(y_m)\left(\delta_{gt}\frac{d^2\phi_l}{dx^2}\zeta_0 - v_x(y_m,z)\frac{d\phi}{dx}\zeta_0\right) \\ &\quad - \sum_{l,n=1}^{L,N} b_{lmn}\psi(y_m)v_x(y_m,z)\frac{d\phi}{dx}\zeta_n + \beta_{gt}\sum_{l,n=1}^{L,N} b_{lmn}\frac{d^2\psi(y_m)}{dy^2}\phi_l\zeta_n + \beta_{gt}\sum_{l=1}^{L} a_{lm}\frac{d^2\psi(y_m)}{dy^2}\phi_l\zeta_0\end{aligned}$$

Eigenfunction expansions are used to approximate all nonhomogeneous terms and all terms whcih are not expressed directly in terms of the eigenfunctions $\psi_l\zeta_n$ from (8). This allows the residual to be written as

$$\begin{aligned}\mathcal{R}(x,y_m,z) &= \psi(y_m)\sum_{l,n=1}^{L,N} b_{lmn}(-\lambda_{ln})\phi_l\zeta_n - \psi(y_m)\sum_{l,n=1}^{L,N} c_{lmn}\phi_l\zeta_n - \psi(y_m)\sum_{l,n=1}^{L,N} f_{lmn}\phi_l\zeta_n \\ &\quad +\beta_{gt}\frac{d^2\psi(y_m)}{dy^2}\sum_{l,n=1}^{L,N} b_{lmn}\phi_l\zeta_n\beta_{gt} + \frac{d^2\psi(y_m)}{dy^2}\sum_{l,n=1}^{L,N} g_{lmn}\phi_l\zeta_n \\ &= \sum_{l,n=1}^{L,N}[\cdots]\,\phi_l\zeta_n.\end{aligned}$$

The mode amplitude coefficients are (for the detailed calculations, please see the Appendix)

$$\begin{aligned}c_{lmn} &= \frac{\delta_{gt}\pi}{2n}(2l-1)^2 + \frac{8v_{max}}{n^3\pi^3}a_l\left(1-(-1)^{2l-1}\right)\left(2+(-1)^n\right)a_{lm} \\ &\quad +\frac{8v_{max}}{n^3\pi^3}\left(2+(-1)^n\right)\sum_{\substack{l=1\\ j\neq l}}^{L} a_{jm}(2j-1)\left(\frac{1-(-1)^{l+j-1}}{l+j-1} + \frac{1-(-1)^{l-j}}{l-j}\right)\end{aligned}$$

$$
\begin{aligned}
f_{lmn} &= 8v_{max}(\frac{1}{3}+\frac{1}{n^2\pi^2})b_{lmn}+16\frac{v_{max}}{\pi^2}\sum_{j}^{L}\sum_{\substack{k=1\\k\neq n}}^{N} b_{jmk}\left(\frac{1+(-1)^{k+n}}{(k+n)^2}-\frac{1+(-1)^{k-n}}{(k-n)^2}\right)\\
&\quad +4v_{max}(\frac{1}{3}+\frac{1}{n^2\pi^2})(2l-1)\sum_{\substack{j=1\\j\neq l}}^{L}\sum_{k=1}^{N} b_{jmk}\left(\frac{1-(-1)^{l+j-1}}{l+j-1}+\frac{1-(-1)^{l-j}}{l-j}\right)\\
&\quad +8\frac{v_{max}}{\pi^2}\sum_{\substack{j=1\\j\neq l}}^{L}\sum_{\substack{k=1\\k\neq n}}^{N} b_{jmk}(2j-1)\left(\frac{1-(-1)^{l+j-1}}{l+j-1}+\frac{1-(-1)^{l-j}}{l-j}\right)\left(\frac{1+(-1)^{k+n}}{(k+n)^2}-\frac{1+(-1)^{k-n}}{(k-n)^2}\right)\\
g_{lmn} &= \frac{2}{n\pi}a_{lm}
\end{aligned}
$$

Projecting the residual onto each trial function $\psi_l\zeta_n$ and setting the resulting equation to zero gives,

$$
\left(\psi(y_m)\lambda_{lmn}-\frac{d^2\psi(y_m)}{dy^2}\beta_{gt}\right)b_{lmn}+\psi(y_m)\sum_{j,k=1}^{L,N} b_{jmk}I_5I_6 = -\psi(y_m)c_{lmn}+\frac{d^2\psi(y_m)}{dy^2}\beta_{gt}g_{lmn}
$$

l=1, ... ,L, n=1, ... ,N

where f_{lmn} is replaced by $\sum_{j,k=1}^{L,N} b_{jmk}I_5I_6$, where I_5, I_6 are defined in the Appendix.

A computationally efficient method for calcualting b_{lmn} is to rearrange each b, c, g, and λ array into column vector format $\mathbf{B}$, $\mathbf{C}$, $\mathbf{G}$, $\mathbf{\Lambda}$, respectively, and reorder the fourth-order tensor, generated by the product of I_5 and I_6, into an array $\mathbf{F}$. This gives

$$
\left[\mathbf{I}\left[\psi(y_m)\mathbf{\Lambda}-\frac{d^2\psi(y_m)}{dy^2}\beta_{gt}\right]+\psi(y_m)\mathbf{F}\right]\mathbf{B}=-\psi(y_m)\mathbf{C}+\frac{d^2\psi(y_m)}{dy^2}\mathbf{G} \tag{12}
$$

where $\mathbf{I}$ is identity matrix. Since there are LMN unknown b_{lmn} coefficients and LMN equations, this linear system can be solved directly to find gas phase temperature, given the flow field characteristics v_{max} and the ratio of the temperature difference between wafer/susceptor and ambient gas to ambient gas temperature C_2.

Results and Discussions

Based on the preceding analysis, representative results are presented for computed gas temperature profile at the centerline of the reactor chamber when the trial function ψ in y direction is selected as $4y(1-y)$. This corresponds to $M=1$ and $y=0.5$. Figure 4 shows the comparison of two temperature profiles computed for the full feed gas flow rate and half that rate. Note that in (a) and (b), only the bottom half of the reactor is

shown since most of the heat transfer occurs in this region and the plots are not propotional in axes. From the temperature contour lines, it is observed that the relatively strong flow field convects most of the energy transferred from the wafer to gas phase out the reactor outlet, limiting the high temperature area to the region above and slightly after the wafer. The benefits of this gas temperature distribution include reduction in undesirable gas phase reactions and the possible formation of contamination particles. Heat transfer rates at the top wafer surface, defined as the heat flux from wafer to the adjacent reactant gas, are shown in Figure 4 (c-d). The heat transfer rates as a function of wafer position can be computed by evaluating the derivatives of the gas temperature at $z = 0$

$$\begin{aligned} q(x,y) = \kappa \left(\frac{\partial T^*}{\partial z^*} \right)_{z=0} &= \kappa \frac{T_{amb}}{2\overline{Z}} \left(\frac{\partial}{\partial z} (T_\Omega + T_{\partial\Omega}) \right)_{z=0} \\ &= \kappa \psi(y_m) \frac{T_{amb}}{2\overline{Z}} \left(\sum_{l,n=1}^{L,N} n\pi b_{lmn} \sin\left(\frac{2l-1}{2} \pi x \right) - \sum_{l=1}^{L} a_{lm} \sin\left(\frac{2l-1}{2} \pi x \right) \right). \end{aligned}$$

In Figure 4 we observe that the enthalpy flux at $z = 0$ is nearly zero over the range of y from the gas inlet to the wafer leading edge. The amount of energy exchanged suddenly jumps to its maximumn value when gas crosses the wafer leading edge. As the gas temperature near the wafer increases, the heat transfer rate slows. After the gas passes the wafer trailing edge, the high temperature gas exchanges energy back to the low temperature chamber wall and results in a positive transfer rate. Gibbs phenomena (Gottlieb and Orszag 1977) resulting from the discontinueous change in gas boundary condition at $z = 0$ is eliminated by a least-squares type linear regression post processing step over the intervals where heat transfer rates are continueous. *It is important to stress that the wiggles seen in T_g near the wafer edge are a true feature of the solution*, and are an indicator of convergence of global trial functions near discontinuities. The enthalpy flux plots show the reduced heat transfer at lower gas velocity, although temperature plots show qualitatively similar contour profiles.

Comparison to Radiative Heat Transfer Rates

In a previous study, a wafer thermal dynamics model (Adomaitis 1997) was developed which accounted for radiative heat exchange between the wafer and chamber walls, heating from the lamp banks, and thermal

conductivity through the wafer been processed:

$$\frac{\partial T_w}{\partial t} = \frac{1}{r}\frac{\partial}{\partial r}\left(r\frac{\partial T_w}{\partial r}\right) + \epsilon_w(1 - T_w^4) + \alpha_w Q.$$

The dimensionless wafer temperature is defined as $T_w = T_w^*/T_{amb}$, radial position $r = r^*/R_w$, and time $t = kt^*/\rho C_p R_w^2$. At steady state, uniform wafer temperature, and vacuum conditions, the wafer temperature equation can be used to determine the energy loss by radiation because the energy provided by the heating lamp will balance radiative energy loss. Assuming a spatially uniform lamp radiant energy distribution and substituting the process parameters into the equation, the radiant energy flux required to maintain a wafer at 600 K is

$$Q = 2\sigma T_{amb}^4(T_w^4 - 1) = 11,174 \quad J/(sec\, m^2)$$

where σ is the Boltzmann's constant = 5.677e-12 $J/(s\ cm^2\ K^4)$. Comparing this result with the heat transfer rate plotted in Figure 4, we conclude that convective heat transfer can not be neglected in this low-pressure system.

Average Heat Transfer Coefficient

Another application of our solution approach is the numerical estimation of an average heat transfer coefficient h, which usually is estimated by collecting experimental data and determining correlations on the basis of dimensional analysis. The heat exchange at the wafer boundary is defined as

$$h(T_{amb} - T_w^*) = \kappa\left(\frac{\partial T_g^*}{\partial z^*}\right)_{z=0}.$$

The total energy transferred from wafer to gas phase can be obtained by integrating the left hand side of this equation over the wafer surface. The average heat transfer coefficient is obtained by dividing the total energy with the temperature difference and surface area. In this case, h equals 2.3998e-4 $J/(m^2Ks)$ for Re = 1167.6.

Solution Convergence

Figures 5 and 6 display the magnitudes of the mode amplitude coefficient a_{lm} and b_{lmn}. The decreasing behavior in both modes of **a** and **b** for increasing mode numbers is a strong indicator of the trial function

expansion convergence. We note that the relative rates of convergence in the b_{lmn} are governed by the eigenvalues, and this relation is shown when we solve the linear system (12). Furthermore, as represented in (9), the eignevalues increase much faster as mode number n increase because the dimensionless parameter γ_{gt} is much larger than δ_{gt}, even though both become larger when mode numbers increase. These different eigenvalue increasing rates result in different convergent rates in the expansion coefficients b_{lmn}, where amplitudes become flat very fast in mode n but the wiggles remain in mode l.

Concluding Remarks

In this paper, a hybird weighted residual method for computing solutions to the flow and temperature fields was developed and applied to a commerical CVD reactor system. The solution procedure developed allows fast and demonstrably accurate analysis of models whose complexity lies in between those can be solved analytically and those must be solved with finite-element packages. We believe one of the primary benifits of this approach is its utility in distinguishing factors which warrant more detailed analysis from those which do not.

Using the procedure developed, the heat transfer rate was calculated explicitly at the wafer/gas boundary. Comparing this convective heat loss from the wafer with the radiative energy losses, the analysis clearly pointed out that convective heat transfer can not be neglected in this low-pressure system. A heat transfer coefficient was estimated from global trial function expansion solution by integrating the heat flux across the wafer. The convergence of the solution was demonstrated by the decreasing mode amplitude coefficients of the eigenfunction solution.

References

[1] Adomaitis, R. A. 1997. An orthogonal collocation technique for rapid thermal processing system discretization. Institute for System Research, University of Maryland, College Park. Technical Report TR97-63

[2] Badgwell, T. A., Breedijk, T., Bushman, S. G., Butler, S. W., Chatterjee, S., Edgar, T. F., Toprac, A. T., and Trachtenberg, I. 1995. Modeling and control of microelectronics materials processing. *Computers Chem. Engng.*, **19**, 1–41.

[3] Duverneuil, P. and Couderc, J. P. 1992. Two-dimensional modeling of low-pressure chemical vapor deposition hot wall tubular reactor. *I. Electrochem. Soc.*, **139**, 296–304.

[4] Gottlieb, D. and Orszag, S. A. 1977. *Numerical Analysis of Spectral Method: Theory and Applications*, 155–157. Society for Industrial and Applied Mathematics, Philadelphia.

[5] Kee, R. J., Dixon-Lewis, G., Warnatz, J., Coltrin, M. E., and Miller, J. 1986. A fortran computer code package for the evaluation of gas-phase multicomponent transport properties. Sandia National Laboratories, Albuquerque / Livermore, Technical Report SAND86-8246.

[6] Kleijn, C. R. 1995. Chemical vapor deposition processes. In Meyyappan, M., editor, *Computational Modeling in Semiconductor Processing*. Artech House, Boston, 97 – 229.

[7] Kleijn, C. R., Hoogendoorn, C. J., Hasper, A., Holleman, J., and Middelhoek, J. 1991. Transport phenomena in tungsten LPCVD in a single-wafer reactor. *J. Electrochem. Soc.*, **138** 509–517.

[8] MacCluer, C. R. 1994. *Boundary Value Problems and Orthogonal Expansions*. IEEE Express, New York, 290–292.

[9] Middleman, S. and Hochberg, A. 1993. *Process Engineering Analysis in Semiconductor Device Fabrication*. McGraw-Hill, 478–573.

[10] Moffat, H. K. and Jensen, K. F. 1988. Three-dimensional flow effects in silicon CVD in horizontal reactors. *J. Electrochem. Soc.*, **135**, 459–471.

Appendix

The unknown coefficients c_{ln}, f_{ln}, and g_{ln} can be found by multiplying both sides of the corresponding equations by $\phi_l \zeta_n$ and integrating over the unit domain.

1. $\psi(y_m)\sum_{j,k=1}^{L,N} c_{jmk}\phi_j\zeta_k = \psi(y_m)\sum_{j=1}^{L} a_{jm}\left(\delta_{gt}\frac{d^2\phi_j}{dx^2}\zeta_0 - v_x\frac{d\phi_j}{dx}\zeta_0\right)$

$$\begin{aligned} c_{lmn} &= 4\sum_{j=1}^{L} a_{jm}\left((\frac{2j-1}{2})\pi\int_0^1 \cos(\frac{2j-1}{2}\pi x)\sin(\frac{2l-1}{2}\pi x)dx\right)\left(4v_{max}\int_0^1 z(1-z)^2\sin(n\pi z)dz\right) \\ &\quad +4\sum_{j=1}^{L} a_{jm}\left((\frac{2j-1}{2})^2\pi^2\delta_{gt}\int_0^1 \sin(\frac{2j-1}{2}\pi x)\sin(\frac{2l-1}{2}\pi x)dx\right)\left(\int_0^1 (1-z)\sin(n\pi z)dz\right) \\ &= 4\sum_{j=1}^{L} a_{jm}I_1I_2 + 4\sum_{j=1}^{L} a_{jm}I_3I_4 \qquad l=1,\ldots,\mathrm{L}, \quad n=1,\ldots,\mathrm{N} \end{aligned}$$

and the four integrals are calculated as follows.

$$\begin{aligned} I_1 &= (\frac{2j-1}{2})\pi\int_0^1 \cos(\frac{2j-1}{2}\pi x)\sin(\frac{2l-1}{2}\pi x)dx \\ &= \begin{cases} \frac{1-(-1)^{2l-1}}{4} & \text{if } j=l \\ \frac{(2j-1)}{4}\left(\frac{1-(-1)^{l+j-1}}{l+j-1}+\frac{1-(-1)^{l-j}}{l-j}\right) & \text{if } j\neq l \end{cases} \end{aligned}$$

$$\begin{aligned} I_2 &= 4v_{max}\int_0^1 z(1-z)^2\sin(n\pi z)dz \\ &= \frac{8v_{max}}{n^3\pi^3}\left(2+(-1)^n\right) \end{aligned}$$

$$\begin{aligned} I_3 &= (\frac{2j-1}{2})^2\pi^2\int_0^1 \sin(\frac{2j-1}{2}\pi x)\sin(\frac{2l-1}{2}\pi x)dx \\ &= \begin{cases} \frac{1}{2}(\frac{2l-1}{2})^2\pi^2 & \text{if } j=l \\ 0 & \text{if } j\neq l \end{cases} \end{aligned}$$

$$\begin{aligned} I_4 &= \int_0^1 (1-z)\sin(n\pi z)dz \\ &= \frac{1}{n\pi} \end{aligned}$$

2. $\psi(y_m)\sum_{j,k=1}^{L,N} f_{jmk}\phi_j\zeta_k = \psi(y_m)\sum_{j,k=1}^{L,N} b_{jmk}v_x\frac{d\psi_j}{dx}\zeta_k$

$$f_{lmn} = 4\sum_{j,k=1}^{L,N} b_{jmk}\left(\int_0^1 (\frac{2j-1}{2})\pi\cos(\frac{2j-1}{2}\pi x)\sin(\frac{2l-1}{2}\pi x)dx\right)\left(4v_{max}\int_0^1 z(1-z)\sin(k\pi z)\sin(n\pi z)dz\right)$$

$$= \quad 4 \sum_{j,k=1}^{L,N} b_{jmk} I_5 I_6 \qquad l{=}1, \, ldots \, ,\mathrm{L}, \quad n{=}1, \, \ldots \, ,\mathrm{N}$$

and

$$I_5 = 4 \int_0^1 (\frac{2j-1}{2})\pi \cos(\frac{2j-1}{2}\pi x) \sin(\frac{2l-1}{2}\pi x) dx$$

$$= \begin{cases} 2 & \text{if } j = l \\ (2j-1)\left(\frac{1-(-1)^{l+j-1}}{l+j-1} + \frac{1-(-1)^{l-j}}{l-j}\right) & \text{if } j \neq l \end{cases}$$

$$I_6 = 4 v_{max} \int_0^1 z(1-z) \sin(k\pi z) \sin(n\pi z) dz$$

$$= \begin{cases} 4 v_{max} (\frac{1}{12} + \frac{1}{4n^2\pi^2}) & \text{if } k = n \\ \frac{2 v_{max}}{\pi^2}\left(\frac{1+(-1)^{k+n}}{(k+n)^2} - \frac{1+(-1)^{k-n}}{(k-n)^2}\right) & \text{if } k \neq n \end{cases}$$

3. $\frac{d^2\psi(y_m)}{dy^2} \sum_{j,k=1}^{L,N} g_{jmk} \phi_j \zeta_k = \frac{d^2\psi(y_m)}{dy^2} \sum_{j=1}^{L} a_{jm} \phi_j \zeta_0$

$$g_{lmn} = 4 \sum_{j=1}^{L} a_j \left(\int_0^1 \sin(\frac{2j-1}{2}\pi x) \sin(\frac{2l-1}{2}\pi x) dx\right) \left(\int_0^1 (1-z) \sin(n\pi z) dz\right)$$

$$= \begin{cases} \frac{2a_l}{n\pi} & \text{if } j = l \\ 0 & \text{if } j \neq l \qquad l{=}1, \, \ldots ,\mathrm{L}, \quad n{=}1, \, \ldots \, ,\mathrm{N} \end{cases}$$

Notation

A_{yz}	area of $y-z$ cross section of gas doamin
$a_{lm}, b_{lmn}, c_{lmn},$	mode amplitude coefficients
$\tilde{d}_{lmn}, f_{lmn}, g_{lmn}$	
B, **C**, **G**, **F**	column vectors for coefficients $b_{lmn}, c_{lmn}, g_{lmn}, f_{lmn}$
C_1, C_2	dimensionless variables of gas temperature boundary conditions
C_p	gas mixture heat capacity, $J/(kg\ K)$
f, g	representative functions to define inner product
h	average heat transfer coefficient, $J/(m^2 Ks)$
I	identity matrix
I_i	i-th integral
I, J, L, M, N	number of modes
$\mathcal{P}$	characteristic pressure drop in x direction, Pa
Q	radiant energy flux, $J/(m^2\ s)$
q	convective energy flux, $J/(m^2\ s)$
$\mathcal{R}$	residual of gas temperature equation
$\mathcal{R}_v$	residual of gas flow equation
R_1	aspect ratio $(=\overline{Y}/\overline{X})$
R_2	radius of suscpetor/wafer $(=R_s/2\overline{X})$
R_s	susceptor diameter, m
R_w	wafer diameter, m
r	radial position of wafer
T_{amb}	ambient inlet tempearture, K
T_g	dimensionless gas temperature
$T_{g,z=0}$	gas temperature boundary condition at $z=0$
T_w	dimensionless wafer temperature
$T_\Omega, T_{\partial\Omega}$	gas temperature defined by (6)
t	dimensionless time
$< v >$	average gas flow velocity in chamber, m/s
v_x	dimensionless gas flow velocity in x-direction.
v_{max}	maximumn gas flow velicity in chamber, m/s
$\hat{v}_x$	gas flow velocity/pressure drop ratio in x-direction
$2\overline{X}$, $2\overline{Y}$, $2\overline{Z}$	characteristic lengths of gas domain, m
x, y, z	streamwise, spanwise, and normal coordinates

Greek

α_v, β_v	dimensionless constants of gas momentum balance equation
α_w	$(= R_w^2\epsilon/(\kappa\Delta_z T_{amb}))$
$\beta_{gt}, \delta_{gt}, \gamma_{gt}$	dimensionless constants of gas energy balance equation
ϵ_w	$(= 2\sigma\epsilon R_w^2 T_{amb}^3/(\kappa\Delta_z))$
η	trial function of gas velocity
κ	gas mixture thermal conductivity
Λ	column vector of eigenvalues
λ	eigenvalues defined by (8)
ϕ, ζ, ψ	trial function components of gas temperature
ζ_0	trial function of gas temperature to avoid vanish at $z=0$
σ	Boltzmann's constant
ρ	gas mixture density
μ	gas mixture viscosity
ξ	normalized trial function of gas velocity

Superscripts

$*$	dimensional quantities

Subscripts

i, j, k, l, m, n	mode numbers

Table 1: Definitions and values of physical properties and dimensionless parameters.

Physical Properties	Value	Dimensionless Parameters	Value
ρ	1.0123 kg/m^3	$\alpha_v = \overline{Y}^2/\overline{Z}^2$	44.4444
κ	0.0168 J/(m K s)	$\beta_v = 2\mathcal{P}\overline{Y}^2/(\mu < v > \overline{X})$	-603.2762
C_p	520.18 J/(kg K)	$\alpha_{gt} = \kappa/(\rho C_p)$	3.1558e-05
μ	2.18e-5 kg /(m s)	$\delta_{gt} = \alpha_{gt}(2 < v > \overline{X})$	1.5829e-04
		$\beta_{gt} = \alpha_{gt}\overline{X}/(2 < v > \overline{Y}^2)$	2.2793e-04
		$\gamma_{gt} = \alpha_{gt}\overline{X}/(2 < v > \overline{Z}^2)$	0.0101

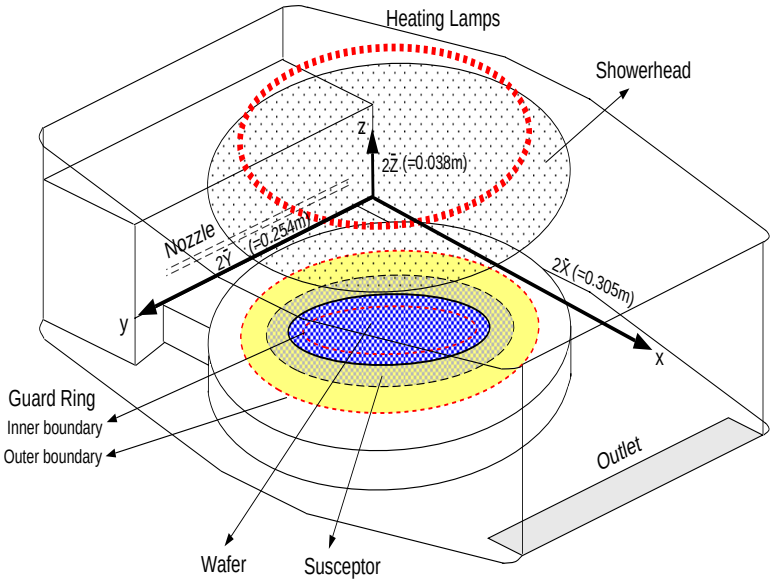

Figure 1: Sketch of the Tungsten CVD reactor system.

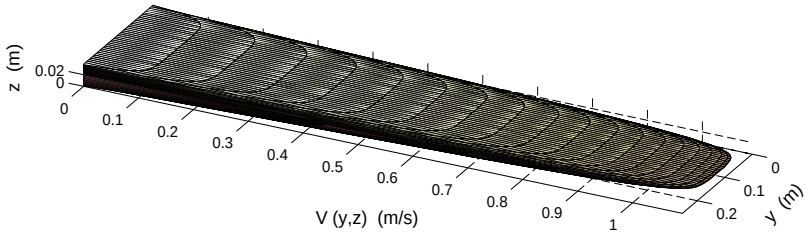

Figure 2: Solution of steady state gas velocity using 16 trial functions in both directions. Re = 1167.6

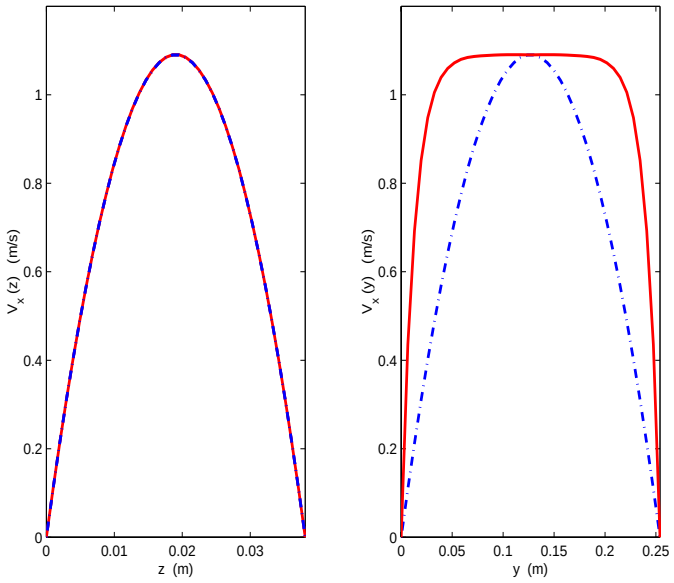

Figure 3: Comparison of flow field calculations. Solid curves correspond to the I = J = 16 term trial function solution. Dashed curves show the single trial function approximation (it lies virtually on top of the solid curve on the left).

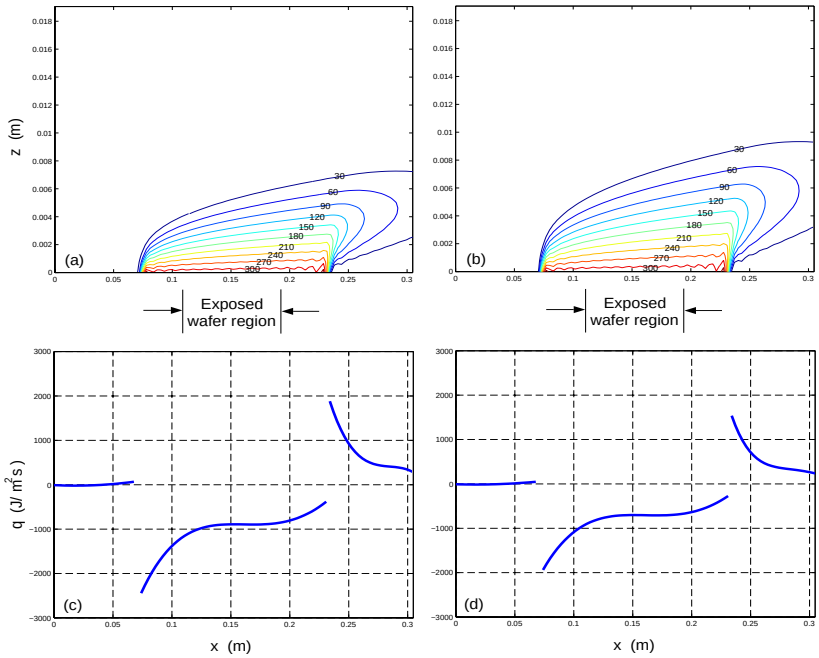

Figure 4: Gas temperature solution and wafer/gas heat transfer rates at centerline of the reactor chamber with different gas flow velocities. Temperature contour lines are labeled in degree C. (a)(c) Simulation performed at Re = 1167.6. (b)(d) Simulation performed at Re = 583.8.

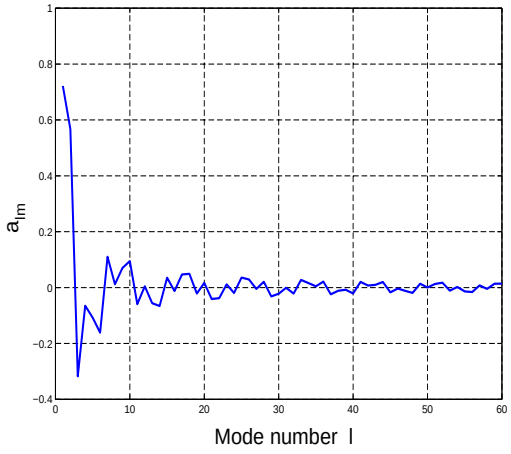

Figure 5: The boundary mode amplitude coefficients a_{lm}.

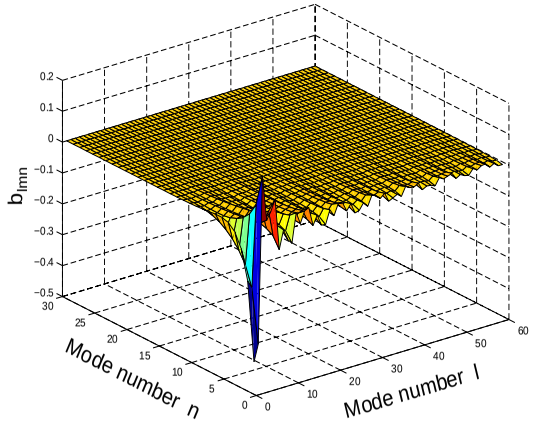

Figure 6: The interior mode amplitude coefficients b_{lmn}.